Springer Proceedings in Physics 140

Thorsten M. Buzug
Jörn Borgert *Editors*

Magnetic Particle Imaging

A Novel SPIO Nanoparticle Imaging Technique

1st Edition

Springer

Springer Proceedings in Physics 140

Springer Proceedings in Physics

Please view available titles in *Springer Proceedings in Physics* on series homepage http://www.springer.com/series/361/

Editors

Thorsten M. Buzug · Jörn Borgert

Magnetic Particle Imaging

A Novel SPIO Nanoparticle Imaging Technique

Springer

Editors
Thorsten M. Buzug
University of Luebeck
Institute of Medical Engineering
Luebeck
Germany

Jörn Borgert
Philips Technologie GmbH
Forschungslaboratorien
Hamburg
Germany

ISSN 0930-8989
e-ISSN 1867-4941
ISBN: 978-3-642-24132-1
e-ISBN: 978-3-642-24133-8
DOI 10.1007/ 978-3-642-24133-8
Springer Heidelberg New York Dordrecht London

Library of Congress Control Number: 2012930496

© Springer-Verlag Berlin Heidelberg 2012
This work is subject to copyright. All rights are reserved by the Publisher, whether the whole or part of the material is concerned, specifically the rights of translation, reprinting, reuse of illustrations, recitation, broadcasting, reproduction on microfilms or in any other physical way, and transmission or information storage and retrieval, electronic adaptation, computer software, or by similar or dissimilar methodology now known or hereafter developed. Exempted from this legal reservation are brief excerpts in connection with reviews or scholarly analysis or material supplied specifically for the purpose of being entered and executed on a computer system, for exclusive use by the purchaser of the work. Duplication of this publication or parts thereof is permitted only under the provisions of the Copyright Law of the Publisher's location, in its current version, and permission for use must always be obtained from Springer. Permissions for use may be obtained through RightsLink at the Copyright Clearance Center. Violations are liable to prosecution under the respective Copyright Law.
The use of general descriptive names, registered names, trademarks, service marks, etc. in this publication does not imply, even in the absence of a specific statement, that such names are exempt from the relevant protective laws and regulations and therefore free for general use.
While the advice and information in this book are believed to be true and accurate at the date of publication, neither the authors nor the editors nor the publisher can accept any legal responsibility for any errors or omissions that may be made. The publisher makes no warranty, express or implied, with respect to the material contained herein.

Printed on acid-free paper

Springer is part of Springer Science+Business Media (www.springer.com)

Preface and Acknowledgements

Magnetic particle imaging is a novel imaging modality which uses various static and oscillating magnetic fields, as well as tracer materials made from iron oxide nanoparticles to perform background-free measurements of the particles' local concentration. The method exploits the non-linear remagnetization behavior of the particles and has the potential to surpass current methods for the detection of iron oxide in sensitivity and spatiotemporal resolution.

This volume is a collection of the accepted contributions of the Second International Workshop on Magnetic Particle Imaging (IWMPI 2012) held at the University of Lübeck, Germany on March 15-16, 2012. The workshop has been organized locally by Medisert, the technology transfer platform of the University of Lübeck, and the Institute of Medical Engineering.

The workshop proceedings cover the status and recent developments in theory and both, instrumentation and tracer materials, as each of them is equally important in designing a well performing MPI. Furthermore, the book aims at presenting first results from phantom and pre-clinical studies.

As workshop chairs we would like to thank the members of the program committee for the selection of the works included in this proceedings: C. Alexiou, University Erlangen; J. Barkhausen, University Clinics Schleswig-Holstein, Campus Lübeck; J. Bulte, Johns Hopkins University, School of Medicine, Baltimore; S. Conolly, UC Berkeley; O. Dössel, University of Karlsruhe; S. Dutz, IPHT Jena; D. Finas, University Clinics Schleswig-Holstein, Campus Lübeck; B. Gleich, Philips Research Hamburg; U. Häfeli, The University of British Columbia, Vancouver; J. Haueisen, Technical University Ilmenau; M. Heidenreich, Bruker BioSpin; U. Heinen, Bruker BioSpin; F. Kießling, University of Aachen (RWTH); T. Knopp, Bruker BioSpin; K. Krishnan, University of Washington; M. Kuhn, Philips Healthcare Hamburg; M. Magnani, Università degli Studi di Urbino; Q. Pankhurst, Davy-Faraday Research Laboratory, London; U.Pison, TOPASS GmbH, Berlin; J. Rahmer, Philips Research Europe – Hamburg; M. Schilling, TU Braunschweig; G. Schütz, Bayer Schering Pharma Berlin; M. Taupitz, Charité Berlin; B. ten Haken, University of Twente; L. Trahms, PTB Berlin; J. B. Weaver, Dartmouth Medical School; J. Weizenecker, University of Applied Sciences Karlsruhe; B. Wollenberg, University Clinics Schleswig-Holstein, Campus Lübeck; Y. Ishihara, Meiji University.

For supporting the workshop we would like to thank the Chamber of Industry and Commerce Lübeck (IHK), Bruker BioSpin, Ettlingen, the cluster agency NORGENTA, Hamburg/Schleswig-Holstein, Philips, Hamburg, LANXESS Deutschland GmbH, Leverkusen und TOPASS GmbH, Berlin, and nanoPET, Berlin, Fork Labs, Lübeck, as well as the German Society for Biomedical Engineering within VDE (DGBMT), the Arbeitsgemeinschaft Medizintechnik (AGMT e.V.), and the EMB section of the IEEE.

Finally, the workshop would not be possible without the work of the local organization team at the University of Lübeck and, especially, Kanina Botterweck. Thank you so much.

March 2012
Lübeck

Thorsten M. Buzug
Jörn Borgert

Contents

Modelling and Simulation Theory

Spectroscopy

Magnetic Particle Separation

Magnetic Nanoparticles

Magnetic Particle Imaging Theory

Medical Applications

Magnetic Particle Imaging

Magnetic Particle Theory

Magneto-Relaxometry

Imaging Technology and Safety Aspects

Short Contributions

Modelling and Simulation Theory

Characterization of Resovist® Nanoparticles for Magnetic Particle Imaging

Takashi Yoshida[1], Keiji Enpuku[1], Frank Ludwig[2], Jan Dieckhoff[2], Thilo Wawrzik[2], Aidin Lak[2], and Meinhard Schilling[2]

[1] Department of Electrical Engineering, Kyushu University,
744 Motooka, Nishi-ku Fukuoka, 819-0395, Japan
`t_yoshi@ees.kyushu-u.ac.jp`
[2] Institut für Elektrische Messtechnik und Grundlagen der Elektrotechnik,
TU Braunschweig, Hans-Sommer-Str. 66, 38106 Braunschweig, Germany
`f.ludwig@tu-bs.de`

Abstract. This study investigates the dynamic magnetic properties of Resovist® for magnetic particle imaging (MPI) utilizing static M-H, ac susceptibility (ACS) and magnetic particle spectroscopy (MPS) measurements on a Resovist® suspension and an immobilized sample. Investigating the magnetic moment and anisotropy energy barrier distributions in the sample as well as the relationship between them, we clarified that the MNPs with large magnetic moment (10^{-24}~10^{-23} Wb·m) and small anisotropy energy barrier play an important role in MPI.

1 Introduction

Resovist® (Bayer Schering Pharma) is the mostly used magnetic nanoparticles (MNP) in MPI since it produces numerous harmonics even for high frequencies of the drive field. It is well recognized that MNPs with large magnetic moment and short relaxation time are suitable for MPI. In previous studies, magnetic properties of Resovist® for MPI were studied, however, without taking account of the relaxation times [1]. Therefore, it is important to quantitatively clarify the dynamic properties of Resovist®. In this study, we first estimate the magnetic moment and anisotropy energy barrier distributions in Resovist® sample as well as the relationship between them. Next, performing a MPS measurement and a numerical simulation on an immobilized sample, we show that MNPs with large magnetic moment and small anisotropy energy barrier in Resovist® particles play an important role in MPI.

T.M. Buzug and J. Borgert (Eds.): Magnetic Particle Imaging, SPPHY 140, pp. 3–7.
springerlink.com

2 Material and Method

Resovist® is a hydrophilic colloidal solution of γ-Fe_2O_3 coated with carboxydextran. Resovist® consists of clusters of single-domain particles as shown in Fig. 1. In this case, the magnetic properties of the MNPs are determined by the magnetic moment, relaxation time, and the dipolar interactions between the single-domain particles in the multi-core particle. Since it becomes, however, very complicated to characterize the magnetic properties taking account of the interactions, we introduce a simple model for multi-core particles as shown in Fig. 1. Briefly, we assume that a multi-core particle has an equivalent magnetic moment m and an equivalent anisotropy energy barrier E_B, which is related to the Néel relaxation time, and behaves like a single-domain particle. In order to estimate the m and E_B distribution which exist in a real sample, we prepared a suspension and an immobilized sample. Both samples contained the same amount of MNPs (418 μg Fe) in the same volume (150 μl). Gypsum was used to immobilize the sample.

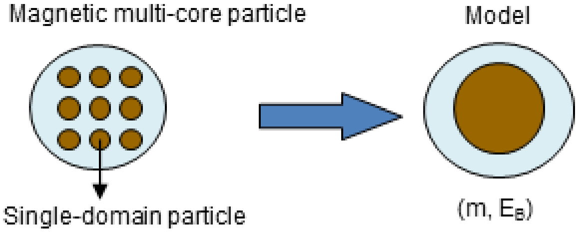

Fig. 1. Analysis model for multi-core particle

3 Estimation of the Anisotropy Energy Barrier and Magnetic Moment Distributions

First, we estimated the E_B distribution from ACS measurement on the immobilized sample. As shown in Fig. 2, the real part of the susceptibility χ'_N of the immobilized sample decreases linearly with ln(f), while its imaginary part χ''_N was almost constant independent of frequency. It can be shown that these dependences occur when the normalized anisotropy energy $\sigma = E_B/k_BT$ of the particles uniformly distributes in the sample. In this case, the complex susceptibility χ_N is given by

$$\chi_N = g_\sigma m^2 \int_{\sigma_1}^{\sigma_2} \left(1 + j\omega\tau_N\right)^{-1} d\sigma = \chi_{Ndc} \left(\sigma_2 - \sigma_1\right)^{-1} \int_{\sigma_1}^{\sigma_2} \left(1 + j\omega\tau_N\right)^{-1} d\sigma , \qquad (1)$$

with a Néel relaxation time of

$$\tau_N = \tau_{0N} \exp(\sigma) = 10^{-9} \exp(\sigma), \qquad (2)$$

where g_σ and χ_{Ndc} is the number density and dc susceptibility of the immobilized sample, respectively. Analyzing χ_N under a constraint that χ_{Ndc} agrees with the dc susceptibility of the suspension sample under small external field [2], the lower and upper values of σ as σ_1=0.26 and σ_2=27 as shown in Fig. 2(b) were obtained.

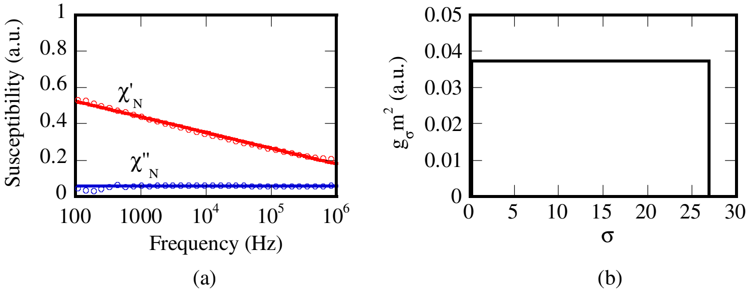

Fig. 2. (a) Frequency dependence of the real χ'_N and imaginary χ''_N parts of the ACS measured on immobilized sample when excitation field amplitude of 95μT was applied. Symbols represent the experimental results, while solid lines represent the calculated ACS for immobilized sample using the obtained anisotropy energy barrier distribution shown in (b).

Next, we estimated the m distribution from a M-H curve measurement on the suspension sample (Fig. 3(a)) using a SVD method [3] . In Fig. 3 (b), the estimated magnetic moment distribution is shown. As can be seen, there are three peaks in $g_m \cdot m^2$, where g_m is the number density. The peak with the highest value of m corresponds to the magnetic moment of multi-core particles, and the other two peaks with small values of m correspond to single-domain particles.

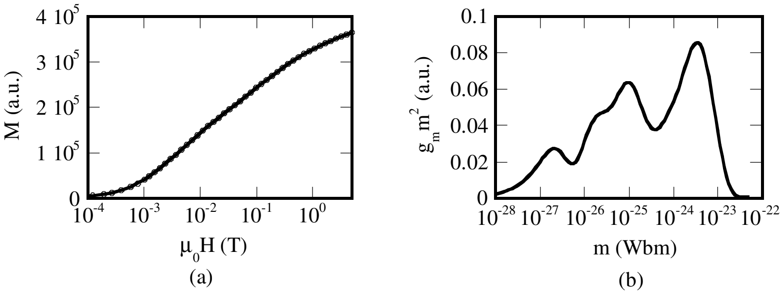

Fig. 3. (a) M-H Curve. Circles represent experimental results, while solid line shows calculated results using the estimated magnetic moment distribution depicted in (b).

Finally, combining the two estimated distributions, i.e., $g_\sigma m^2$-σ and $g_m m^2$-m, the relationship between σ and m was estimated. As shown in Fig. 4, there are three types of MNPs in Resovist®: Type-I MNPs with small m and small σ. Type-II MNPs with large m and small σ. Type-III MNPs with large m and large σ. The fraction of type-II MNPs with large m (10^{-24}~10^{-23} Wb·m) and small σ ($\tau_N=10^{-8}$~1 s) was 34% in terms of $g_m m$.

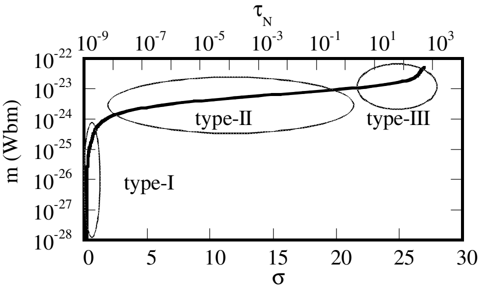

Fig. 4. Relationship between magnetic moment and anisotropy energy barrier.

4 Harmonics Spectrum

When the MNPs are used to bind to a target of interest inside the body in MPI application, MNPs are physically immobilized. In this case, relaxation and magnetization occur via the Néel mechanism. Therefore, one of the important characteristics of MNPs in MPI is the harmonics spectrum on immobilized sample. In Fig. 5, the harmonics spectra of the immobilized Resovist® sample are shown, when a field amplitude of 20 mT_{rms} with 1 kHz or 10 kHz was applied. As can be seen, the harmonics spectrum has a frequency-dependence due to the Néel relaxation.

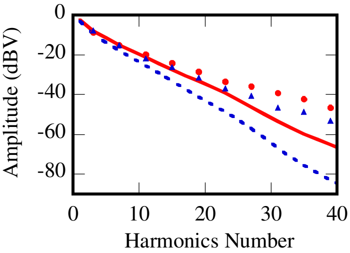

Fig. 5. Harmonics spectra of immobilized Resovist® sample when field amplitude of $20mT_{rms}$ was applied. Circles and triangles represent the experimental results with drive frequency of 1 kHz and 10 kHz, respectively. Solid and dashed lines represent the simulation results with drive frequency of 1 kHz and 10 kHz, respectively.

In order to make a comparison between the experimental and theoretical harmonics spectra, we performed MPS simulations for the immobilized sample using the estimated distributions as shown in Fig. 2(b) and 3(b) as well as the relationship between m and σ as shown in Fig. 4. In this MPS simulation, we solved the following Fokker-Planck equation:

$$2\tau_N \sin\theta \frac{\partial W}{\partial t} = \frac{\partial}{\partial \vartheta}\left\{\sin\theta\left(\frac{1}{k_B T}\frac{\partial E}{\partial \theta}W + \frac{\partial W}{\partial \theta}\right)\right\} + \frac{\partial}{\partial \vartheta}\left(\frac{1}{\sin\theta}\frac{\partial W}{\partial \phi}\right), \tag{3}$$

with

$$E = -mH\cos(\omega t)\cos\theta . \tag{4}$$

This equation is applicable for Néel particles when σ is small [4]. In order to take into account of the σ-dependent Néel relaxation time, we used the σ-dependent Néel relaxation time τ_N given by eq. (2). As shown in Fig. 5, the simulated harmonic spectrum reasonably agreed with the measured results for lower harmonics, though the simulated results became smaller than the experimental ones for higher harmonics. From the numerical simulation, we found that roughly 90% of the 3rd harmonic signal was generated from type-II MNPs with large m (10^{-24}~10^{-23} Wb·m) and small σ (τ_N=10^{-8}~1 s).

5 Conclusion

Investigating the magnetic moment and anisotropy energy barrier distributions in Resovist® particles as well as the relationship between them, we clarified that the harmonics spectrum is mainly generated by the MNPs with large magnetic moment (10^{-24}~10^{-23} Wb·m) and small anisotropy energy barrier (τ_N=10^{-8}~1 s), whose relative portion is roughly 30% in terms of number times magnetic moment.

We thank Dr. D. Eberbeck of PTB for measuring the M-H curve. Financial supports from the DFG via SFB 578, the European Commission Framework Programme 7 under the NAMDIATREAM project (No. NMP-2010-246479), the JSPS Institutional Program for Young Researcher Overseas Visits, and the JSPS via Grant-in-Aid for Young Scientists (B) (23760369) are acknowledged.

References

1. Biederer, S., et al.: Magnetization response spectroscopy of superparamagnetic nanoparticles for magnetic particle imaging. J. Phys. D: Appl. Phys. 42, 205007 (2009)
2. García-Palacios, J.L., Lázaro, F.J.: Langevin-dynamics study of the dynamical properties of small magnetic particles. Phys. Rev. B 58, 14937–14958 (1998)
3. Berkov, D.V., et al.: New method for the determination of the particle magnetic moment distribution in a ferrofluid. J. Phys. D 33, 331–337 (2000)
4. Coffey, W.T., Cregg, P.J., Kalmykov, Y.P.: In: Prigogine, I., Rice, S.A. (eds.) Advances in Chemical Physics, vol. 83, p. 263. Wiley, New York (1993)

Nonlinear Behavior of Magnetic Fluid in Brownian Relaxation: Numerical Simulation and Derivation of Empirical Model

Takashi Yoshida and Keiji Enpuku

Department of Electrical Engineering, Kyushu University, University Name,
744 Motooka, Nishi-ku Fukuoka, 819-0395, Japan
t_yoshi@ees.kyushu-u.ac.jp

Abstract. Nonlinear Brownian relaxation of magnetic fluids for the case of large excitation field was studied in relation to its biomedical applications. The Fokker-Planck equation, which describes the nonlinear behavior of magnetic fluids, was solved by numerical simulation when ac field was applied. Frequency-dependences of the harmonics were investigated in terms of the effective Brownian relaxation time τ_{eff}, which was empirically obtained from the ac susceptibility of the fundamental component. It was shown that higher harmonics become small even at $\omega\tau_{\mathrm{eff}}=1$ compared to each quasi-static harmonics amplitudes.

1 Introduction

Magnetic nanoparticles (MNPs) have been widely studied for biomedical applications. In many cases, MNPs are used in a suspension, i.e., magnetic fluids. One important property of magnetic fluids is Brownian relaxation. It is well-known that this property can be represented by Debye model in linear regime, i.e., for small excitation field. On the other hand, nonlinear properties of the Brownian relaxation appear under large excitation field, such as the decrease in ac susceptibility and the occurrence of the higher harmonics [1]. Recently, these nonlinear properties have been used for magnetic particle imaging [2] and immunoassay [3]. Therefore, it is important to quantitatively characterize the nonlinear Brownian properties for biomedical applications.

2 Numerical Simulation

We studied nonlinear behavior of the magnetic fluid in Brownian relaxation when ac field was applied. For the case of spherical single-domain particles,

T.M. Buzug and J. Borgert (Eds.): Magnetic Particle Imaging, SPPHY 140, pp. 9–13.
springerlink.com

the behavior of magnetic fluids can be described by the Fokker-Planck equation [1]:

$$2\tau_{\mathrm{B}}\frac{\partial W(\theta,t)}{\partial t}=\frac{1}{\sin\theta}\frac{\partial}{\partial\theta}\left\{\sin\theta\left[\xi\cos(\omega t)\sin\theta\cdot W(\theta,t)+\frac{\partial W(\theta,t)}{\partial\theta}\right]\right\}, \quad (1)$$

where θ is the angle of the magnetic moment *m* with respect to the applied field of $H_{ac}=H\cos(\omega t)$, $W(\theta,t)$ is the distribution function of *m*, $\xi = mH/k_BT$ is the ratio of external field energy to the thermal energy k_BT. τ_B is the Brownian relaxation time given by $\tau_B=3\eta V/k_BT$, where η is the viscosity of the fluid, *V* is the volume of the particle. We obtain the distribution function $W(\theta,t)$ solving eq. (1) with numerical simulation. Then, we can calculate the mean magnetic moment <*m*> in the direction of the applied field by

$$\langle m\rangle/m=\int_0^{\pi}W(\theta,t)\sin\theta\cos\theta d\theta\,. \quad (2)$$

3 Simulation Results and Discussion

Harmonic signals from the magnetic fluids are detected to reconstruct the space distribution of the magnetic fluids in MPI application [2]. Harmonic spectrum in ac field is also used to characterize the magnetic properties [4]. Therefore, it is important to quantitatively clarify the frequency-dependence of the harmonic spectrum. In Fig. 1, numerical simulation results of the harmonic amplitudes in quasi-static case, i.e., when the frequency approaches zero, are shown. The values of $m_k(0)$ (k=1 - 11) are shown for various field amplitudes of ξ=2, 5, and 20. Here k is the harmonics number. As shown, harmonic spectrum has strong dependence on the field amplitude.

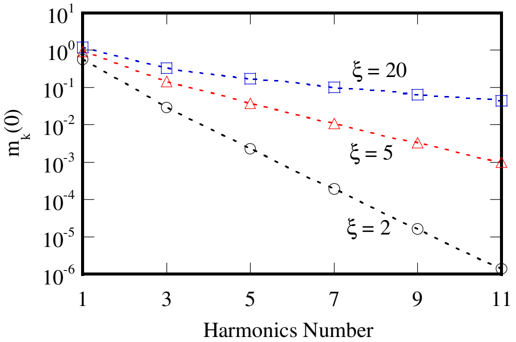

Fig. 1. Harmonic spectra for quasi-static case when various field amplitude of ξ = 2, 5, and 20 are applied. Symbols represent the numerical simulation results, while dashed lines represent the theoretical spectra, which are obtained by the Fourier expansion of the Langevin function.

In Fig. 2, frequency dependences of the harmonic amplitudes normalized by each quasi-static amplitude, i.e., $|m_k(\omega)|/m_k(0)$, are shown. As shown, frequency dependences of the normalized harmonic amplitudes are not the same, but strongly depend on the harmonic number k.

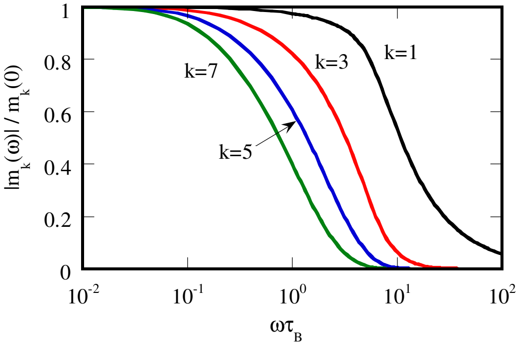

Fig. 2. Frequency-dependences of the harmonic amplitudes normalized by each quasi-static amplitude.

Next, we study the ac susceptibility of the fundamental component in order to explore the field-dependence and frequency-dependence of the nonlinear properties of the magnetic fluids. In Fig. 3, the frequency dependences of the real (χ'_1) and imaginary (χ''_1) parts of the susceptibility are shown. As shown in Fig. 3(b), ac susceptibility becomes different from the Debye equation when the field becomes large, i.e., for the case of ξ=10. For example, the frequency f_p at which χ''_1 has a peak value becomes higher when ξ =10.

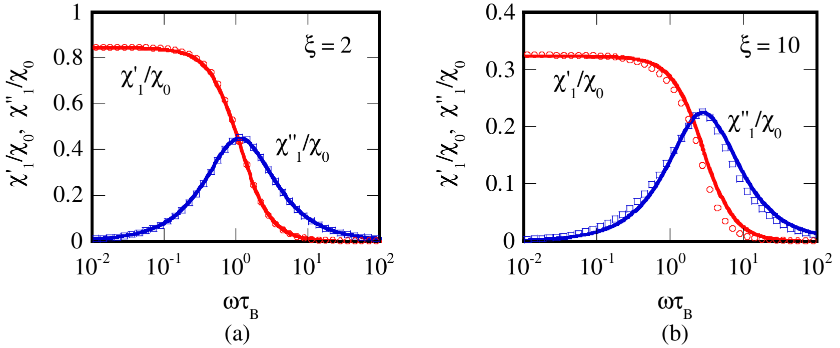

(a) (b)

Fig. 3. Frequency dependences of the real (χ'_1) and imaginary (χ''_1) parts of the susceptibility of the fundamental component for ac excitation fields. (a) ξ=2 and (b) ξ=10. Symbols represent simulation results, while solid lines are obtained from eqs. (3) and (4).

In order to obtain empirical equations that can explain the simulation results, we modified the Debye equation as:

$$\chi'_1(\omega)/\chi_1(0)=1/\left[1+(\omega\tau_{\mathrm{eff}})^2\right], \tag{3}$$

$$\chi''_1(\omega)/\chi_1(0)=k''(\xi)\omega\tau_{\mathrm{eff}}/\left[1+(\omega\tau_{\mathrm{eff}})^2\right], \tag{4}$$

with

$$\chi_1(0)/\chi_0=1-\xi^3/\left(10+9\xi+3.81\xi^2+\xi^3\right), \tag{5}$$

$$\omega_{\mathrm{p}}=2\pi f_{\mathrm{p}}=1/\tau_{\mathrm{eff}}=\sqrt{1+0.07\xi^2}/\tau_{\mathrm{B}}, \tag{6}$$

$$k''(\xi)=1+0.024\xi^2/\left(1+0.18\xi+0.033\xi^2\right). \tag{7}$$

Here, $\chi_1(0)$ is the susceptibility in the quasi-static case, $\chi_0 = \mu_0 M_s^2 V/(3k_B T)$ is the dc susceptibility for small fields, M_s is the saturation magnetization. Simulation results of $\chi_1(0)/\chi_0$ and the effective relaxation time τ_{eff}, given by $\tau_{\mathrm{eff}}=1/\omega_p$, are shown in Fig. 4. As shown in Fig. 4(a), $\chi_1(0)/\chi_0$ decreased with ξ, which indicates a decrease in the susceptibility at large fields. Effective relaxation time τ_{eff} also decreased with ξ as shown in Fig. 4(b). Dependences of $\chi_1(0)$ and τ_{eff} on ξ can be well expressed with eqs. (5) and (6).

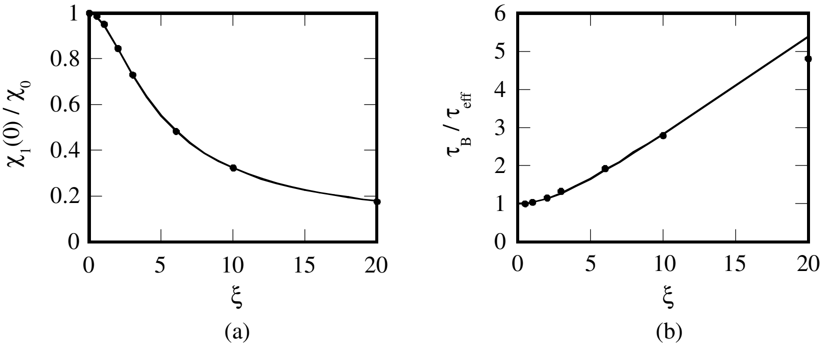

Fig. 4. (a) Dependence of $\chi_1(0)$ on ξ. Circles are simulation results, while the solid line is obtained from eq. (5). (b) Effective Brownian relaxation time τ_{eff} for ac fields. τ_{eff} is determined from the frequency f_p at which χ''_1 shown in Fig. 3 has a peak value. Circles are simulation results, while the solid line is obtained from eq. (6).

Finally, we explore the frequency dependences of $|m_k(\omega)|/m_k(0)$ by taking into account the effective relaxation time τ_{eff} given by eq. (6). In Fig. 5, frequency dependences of $|m_k(\omega\tau_{\mathrm{eff}})|/m_k(0)$ are shown when ξ=20. Note that the horizontal axis depicts the angular frequency normalize by $1/\tau_{\mathrm{eff}}$, i.e., $\omega\tau_{eff}$. As can be seen, frequency dependence becomes stronger for larger harmonic number k. For example, at the frequency of $\omega\tau_{eff}=1$, the value of $|m_k(\omega\tau_{eff})|/m_k(0)$ becomes 0.8, 0.27, 0.06, and 0.0094 for the harmonic number of k=1, 3, 5 and 7, respectively. On the other hand, if we obtain the same amplitude of $|m_k(\omega\tau_{eff})|/m_k(0)=0.8$, the frequency should be $\omega\tau_{eff}=1$, 1/4.9, 1/12, and 1/21 for k=1, 3, 5 and 7, respectively. This result indicates the rapid decrease of the harmonic signals at high frequencies. Therefore, these frequency dependences of the higher harmonics should be taken into account when they are used.

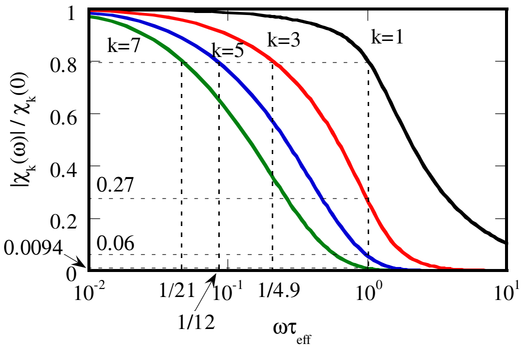

Fig. 5. Comparison of the frequency-dependences of the harmonic amplitudes.

4 Conclusion

The nonlinear Brownian relaxation of magnetic fluids was studied by numerically solving the Fokker-Planck equation. Nonlinear properties such as field-dependent effective relaxation time τ_{eff} and susceptibilities were clarified quantitatively. It was shown that the frequency dependence of the harmonic signal became stronger for larger harmonic number, resulting in the significant decrease in the signal even at $\omega\tau_{eff}=1$. These frequency dependences of the higher harmonics should be taken into account when they are used.

References

1. Yoshida, T., Enpuku, K.: Simulation and Quantitative Clarification of AC Susceptibility of Magnetic Fluid in Nonlinear Brownian Relaxation Region. Jpn. J. Appl. Phys. 48, 127002 (2009)
2. Gleich, B., Weizenecker, J.: Tomographic imaging using the nonlinear response of magnetic particles. Nature 435, 1214–1217 (2005)
3. Nikitina, P.I., Vetoshko, P.M., Ksenevich, T.I.: New type of biosensor based on magnetic nanoparticle detection. J. Magn. Magn. Mater. 311, 445–449 (2007)
4. Biederer, S., et al.: Magnetization response spectroscopy of superparamagnetic na-noparticles for magnetic particle imaging. J. Phys. D: Appl. Phys. 42, 205007 (2009)

Magnetic Particle Imaging Using Ferromagnetic Magnetization

Stephan Euting[1], Fernando M. Araújo-Moreira[2], and Waldemar Zylka[1]

[1] Department of Physical Engineering, Westfälische Hochschule
Neidenburger Str. 43, Gelsenkirchen, 45877, Germany
`euting@medicalengineer.de, waldemar.zylka@fh-gelsenkirchen.de`
[2] Department of Physics, Federal University of São Carlos (UFSCar)
Via Washington Luis, km 235, Caxia postal 676, São Carlos, 13565-905, Brazil
`faraujo@df.ufscar.br`

Abstract. Nanofluids, defined as fluids containing suspended solid nanoparticles, are potential systems for utilization in biomedical applications. Magnetic Particle Imaging (MPI) uses superparamagnetic nanofluids, e.g. a colloidal suspension of iron oxide particles. In this work a new biocompatible nanofluid based on pure and stable ferromagnetic carbon is investigated. Although this material has a relatively small value of coercive magnetic field, it does exhibit a true ferromagnetic behavior up to 300 K. We present results obtained from numerical investigations performed to calculate the impact of a ferromagnetic magnetization to the MPI signal chain. Moreover, by modeling ferromagnetic magnetization we prove here the general suitability of ferromagnetic materials for MPI. Due to the low saturation magnetization, however, MPI for ferromagnetic carbon will be possible only in the near future when realistic concentrations of the nanofluid ferromagnetic carbon will be experimentally obtainable.

1 Introduction

The members of the class of materials called magnetic can be classified by their magnetization and/or their magnetic susceptibility to an applied magnetic field into *diamagnetic*, *paramagnetic*, and *ferromagnetic* materials. *Superparamagnetism* is a form of magnetism which appears in ferromagnetic nanoparticles, among other types of magnetic materials. If those nanoparticles are sufficiently small, the magnetization can randomly flip its direction under the influence of temperature. The magnetization curve of the assembly as a function of the applied magnetic field is a reversible S-shaped curve.

Potential nano-systems for uses in biological and medical applications are the so-called nanofluids defined as fluids containing suspended solid nanoparticles with different sizes. A most recognizable class of magnetically

T.M. Buzug and J. Borgert (Eds.): Magnetic Particle Imaging, SPPHY 140, pp. 15–20.
springerlink.com

controllable nanofluid simultaneously exhibiting both fluid and magnetic properties is the ferrofluid, a suspended colloidal fluid of nanosized iron oxide (Fe3O4 or g-Fe2O3) particles frequently called SPIO. When used in MPI the nanoparticles are sufficiently small and the ferrofluid suspension became superparamagnetic [1].

Instead of ferrofluids, a new nanofluid based on pure ferromagnetic carbon is investigated as contrast material for MPI in this paper. Carbon materials, especially nanocarbons, constitute one of the most fascinating classes of structures, exhibiting a wide variety of forms and properties. The possibility of achieving striking properties in macroscopic carbon - such as room-temperature magnetic properties and even superconductivity – is attracting the scientific community and open up a plethora of possible applications of this material in engineering, as well as in medicine and biology, as a biocompatible magnetic material.

While the basic research of the ferromagnetic carbon is in progress, a model describing ferromagnetic magnetization is already available [5]. This allows studying the suitability of ferromagnetic materials, e.g. nanofluid ferromagnetic carbon, in MPI.

2 Material and Methods

2.1 Ferromagnetic Graphite and Nanofluid Magnetic Carbon

Ferromagnetic carbon can be produced by a vapor phase redox reaction in closed nitrogen atmosphere with copper oxide (CuO) [2,3]. Recent theoretical and experimental reports confirm that magnetic carbon is originated from defects [6-9]. In the present case, those defects are introduced into the carbon structure by the vapor phase redox reaction. Atomic and magnetic force microscopy (AFM/MFM) can be used to study the presence of magnetic regions which are approximately 1μm.

The chemical route for synthesizing nanofluid magnetic carbon (NFMG) is described in [4]. The structural characterization can be performed by transmission electron microscopy (TEM) leading results shown in Fig. 1, revealing a flake-like morphology. Relating the size of the scale in Fig. 1 (left) with the size of the particle in the nanofluid, the latter is estimated to be of the order of 10nm.

Besides, according to Fig. 1 (right), which shows M-H curves at 2 and 300K, the hysteresis does not disappear with increasing temperature and manifests itself in nonzero values of remnant magnetization and coercive magnetic field. Consequently, we can conclude that, even though the NFMG nanofluid has a relatively small value of coercive magnetic field (quasi-superparamagnetic state), it does exhibit a true ferromagnetic behavior up to 300K.

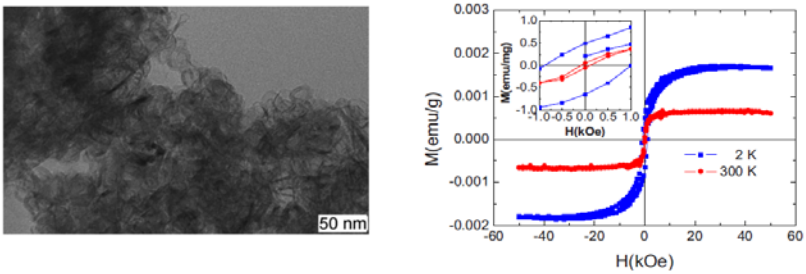

Fig. 1. Left: TEM image of NFMG sample showing a flake-like structure with an average size of the particle of the order of 10 nm. Right: The hysteresis curves for NFMG sample for two temperatures 2 and 300 K showing a ferromagnetic like behavior of the sample. Inset: low-field M-H curves.

The stability of NFMG can be verified by Zeta potential measurements of the nanoparticles under suspension. The Zeta potential indicates the level of the repulsion between particles similarly charged in dispersion. This means that the higher the Zeta potential, the more the dispersion will resist to aggregation, resulting in a longer period of stability. The stability of the dispersed solution of NFMG associated to its magnetic features, confirms its potential to be used in biological and medical applications, like imaging specifically MPI.

2.2 MPI Using Ferromagnetic Magnetization

Numerical investigations of a MPI systems using superparamagnetic nanofluid demonstrated, among others, good resolution and high sensitivity [10], field free line feasibility for signal encoding [11] even for different trajectories and trajectory densities [12]. To compare simulation results of a superparamagnetic versus a ferromagnetic nanofluid a two dimensional MPI setup similar to [12] is implemented. Two perpendicular Maxwell coil pairs, diameter of $D=500mm$, are generating the selection and driven field. The distance between the coil and its opponent is $1000mm$. The size central field of view is $30mm$ x $15mm$. The Biot-Savart law is solved for the sensitivity profile using elliptic integrals [13] and a current strength of $I=1A$. In turn, the sensitivity profile is used to calculate induced voltages. The gradient strengths are $dH_z/dz=2.5T/\mu_0 m$ and $dH_x/dx=1.25T/\mu_0 m$.

Frequently the well-known Langevin function for the anhysteretic S-shaped magnetization M_{an} is used to model a superparamagnetic magnetization [10]. In contrast, the ferromagnetic behavior can be expressed by the differential equation [5]:

$$\frac{dM_{hyst}}{dH} = \frac{1}{(1+c)}\frac{1}{\delta k/\mu_0 - \alpha\left(M_{an} - M_{hyst}\right)}\left(M_{an} - M_{hyst}\right) + \frac{c}{(1+c)}\frac{dM_{an}}{dH}.$$

Here H is the magnetic field while H_e (occurring in the Langevin function) is the effective magnetic field given by $H_e = H + \alpha M_{hyst}$, where α denotes a mean field parameter representing inter-domain coupling. The coefficient c describes the ratio of the initial differential susceptibilities of the normal and the anhysteretic magnetization curves, $c = \chi'_{0norm} / \chi'_{0anhy}$ which can be measured experimentally. The parameter k is called shape forming parameter; μ_0 is the permeability in free space and δ takes the value $+1$ if H increases, $dH/dt > 0$ and -1 if H decreases, $dH/dt < 0$. Implicit parameters of the magnetization M_{an} are: M_s the saturation magnetization, $a = (k_B T)/(\mu_0 m)$ with k_B the Boltzmann constant, T the temperature in Kelvin, and m the magnetic moment of a particle. We solved the differential equation implementing a standard 4th order Runge-Kutta method [14].

The image reconstruction, i.e. solution of the equation $\hat{\mathbf{G}}\mathbf{c} = \hat{\mathbf{u}}$, for $\mathbf{c}$, where $\hat{\mathbf{G}}$ is the one dimensional discrete Fourier transformed system matrix, $\mathbf{c}$ the unknown concentration and $\hat{\mathbf{u}}$ the Fourier transformed induced voltage, is obtained by a combination of singular value decomposition and Tikhonov regularization. The regularization parameter suggested in [10] is used.

To compare MPI results for superparamagnetic versus ferromagnetic nanofluids, parameters from [12] are adopted: For the superparamagnetic nanofluid, the saturation magnetization is $M_s=477\text{x}10^3 A/m$ and $a=505.06\ A/m$. Those values are used for the ferromagnetic nanofluid too and, in addition, the following values to form an adequate hysteresis curve: $k=1.6\text{x}10^3 Vs/m^2$, $\alpha=1.6\text{x}10^{-3}$, $c=0.01$.

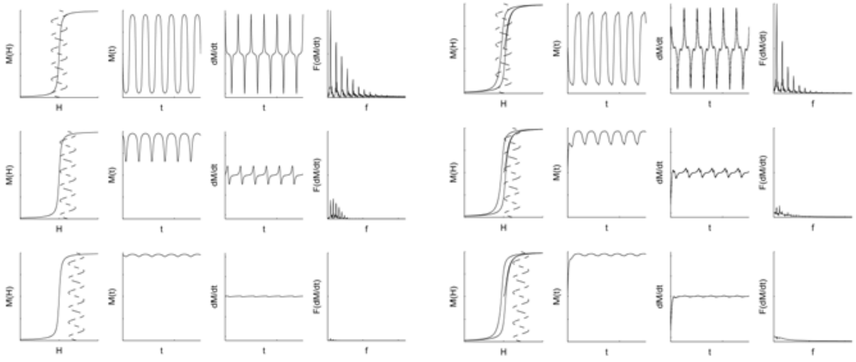

Fig. 2. Comparison of MPI signals chain for three different offset fields using superparamagnetic (left) and ferromagnetic nanofluid (right).

3 Results

Figure 2 shows the MPI signal chain for superparamagnetic and ferromagnetic particles for various values of the offset field: Magnetization, induced voltage, and frequency spectrum. In both magnetization classes, higher